Available online at www.sciencedirect.com
SCIENCE DIRECT®
International Journal of Heat and Fluid Flow 25 (2004) 481–488
International Journal of HEAT AND FLUID FLOW
www.elsevier.com/locate/ijhff

Effect of bubble diameter on modification of turbulence in an upward pipe flow

Akiko Fujiwara [a,*], Daijyu Minato [b], Koichi Hishida [b]

[a] Intelligent Modeling Laboratory, The University of Tokyo, 7-3-1 Hongo, Bukyo-ku, Tokyo 113-8656, Japan
[b] Department of System Design Engineering, 3-14-1 Hiyoshi, Kohoku-ku, Yokohama 223-8522, Japan

Abstract

The experimental study in vertical upward driven bubbly pipe flow with void fractions of 0.5% and 1.0% is conducted to elucidate the effect of dispersed bubble size on turbulence modification. Liquid phase velocity is measured by particle image velocimetry with fluorescent tracer particles (PIV/LIF). Bubble size and velocity are estimated from the bubble image observed by a projected shadow image technique. Bubbles strongly accumulate near the wall which accelerate the liquid phase. The high concentration of bubbles in the vicinity of the wall induces a reduction of the fluctuation velocity intensity of the liquid. The effect of bubble-induced turbulence on the global pipe flow structure was investigated by the turbulence energy production and dissipation, estimated from the experiment data, and local vortical structure around the bubbles.

Keywords: Bubbly pipe flow; Turbulence energy budget; Instantaneous vorticity fluctuation

1. Introduction

The greatest interest in the multiphase flow is the interaction of the dispersed phase with the underlying turbulent flow. Knowledge of bubbly flows is significant to different engineering systems such as chemical reactors and power plant. In addition, there is interest in frictional drag reduction by micro-bubble injection around ship hulls in the field of marine engineering. In order to gain further knowledge of the effect of bubbles on turbulence modification, various experimental and numerical studies have been conducted. In gas–liquid bubbly flows, past experiments in pipe flow indicated that turbulence augmentation and reduction depends on the void fraction and gas flow rate (Serizawa et al., 1975; Theofanous and Sullivan, 1982; Wang et al., 1987; Lance and Bataille, 1991). There is some discrepancy of tendency on the turbulence modification by bubbles even for similar conditions.

From the point of view of the numerical study, Lain et al. (2002) proposed the numerical model of turbulent bubbly flow using an Euler/Lagrangian approach. They coupled the k–ε turbulence model and a dispersed bubble motion of equation simulated within a Lagrangian framework. They applied this coupled methodology for a simple pipe flow situation, and obtained good agreement with experimental data. Bunner and Tryggvson (2002, 2003) reported the precise direct numerical simulations study of the three-dimensional deformable buoyant bubbles in a homogeneous flow. They adopted a parallelized finite-difference/front tracking method to calculate the deformable gas–liquid interface. They obtained the effect of the void fraction on the fluctuation velocity, the effect of bubble motion caused by bubble deformation, and the kinetic energy spectrum. These numerical studies suggested the feasibility of performing the simulations of large systems of dispersed bubbly flows to complement experiments and assist to develop new modeling.

Recently it has been attempted to apply particle image velocimetry (PIV) technique to the dispersed two-phase flow. This technique has advantages, those are, it is non-contact measurement and does not disturb the flow structure, and the spatial interaction between the

* Corresponding author. Tel.: +81-3-5841-6288; fax: 81-3-5841-8542.
E-mail addresses: fujiwara@fel.t.u-tokyo.ac.jp (A. Fujiwara), minato@mh.sd.keio.ac.jp (D. Minato), hishida@sd.keio.ac.jp (K. Hishida).

0142-727X/$ - see front matter © 2004 Elsevier Inc. All rights reserved.
doi:10.1016/j.ijheatfluidflow.2004.02.018

dispersed and the continuous phases is obtained in time series. Sato and Hishida (1996) adopted the PIV technique to dispersed liquid–solid two-phase flow, and discussed the turbulence energy budget balance and the effect of an extra force term which is induced from the particle drag force. Also they reported the correlation between the local enstrophy distribution and the local shear flow structure at inter-particle spacing distorted by the particles (Sato and Hishida, 2000). For the gas–liquid two-phase flow, Murai et al. (2000) introduced the PIV measurement for the bubbly channel flow. They experimentally verified the inverse turbulence energy cascade. Nevertheless the correlation between the local turbulence structures in bubbly flow and the global turbulent modification is still not explored by experiment. The detailed information on a local structure of turbulence modification has been demanded by reliable experiments. That is, local turbulence structure and its relation to global turbulence characteristics must be given by an advanced type of experimental technique.

The objective of this study is to elucidate the structure of turbulence modification in terms of bubble diameter in a fully developed pipe flow. Specifically, we aim to deduce the correlation between the global turbulence flow structure and the local turbulence modification induced by the presence of bubbles and as characterized by the instantaneous vorticity from experimental results. Moreover we discuss the local vortical flow structure around the bubbles by an estimation of the fluctuation vorticity intensity obtained from PIV applied LIF measurements.

2. Experimental method

2.1. Measurement technique

In order to measure the flow structure around the bubbles, specifically to detect the interaction between the bubble motion and the flow field, we applied the PIV/LIF system with Rhodamine-B, a fluorescent dye previously described by Tokuhiro et al. (1998). Fig. 1 shows the measurement systems. The particles are excited by a Nd:YVO_4 laser sheet ($\lambda = 532$ nm), and fluorescence emission in the vicinity of the bubbles is detected through a color filter (which cuts off the reflection) attached to a CCD camera (left camera image). Two-dimensional velocity vector fields are obtained in time. The experimental error associated with the present PIV system is estimated to be 4.3% at 95% confidence limits.

In order to capture the simultaneous shape and position of bubbles, the projected shadow image technique (Tokuhiro et al., 1998) is applied using blue ($\lambda = 470$ nm) LEDs as the light source. In Fig. 1 (right camera image) bubbles are illuminated from behind, and depicted in terms of a grayscale background. The focal depth of the CCD camera is approximately 6 mm. Bubbles in this field have been captured at a single instance in time. The emitted light passes through a filter attached to the CCD camera, which records the shadow image. The procedure for the detection of bubble shape and position is given below.

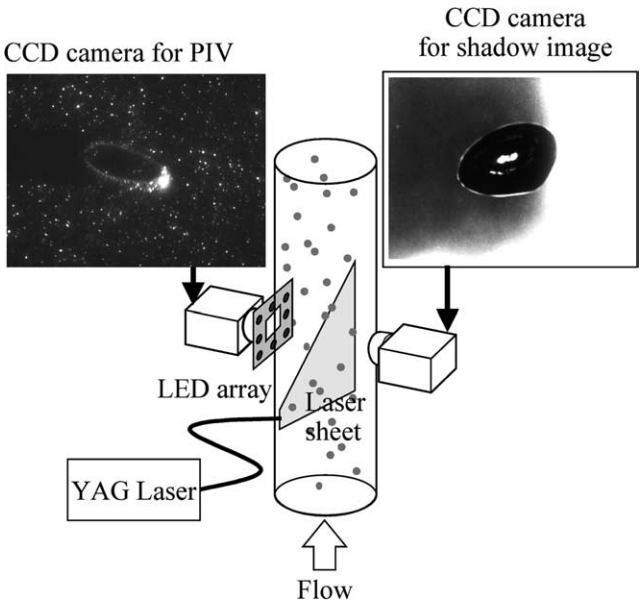

Fig. 1. Schematic of measurement system.

(1) The background image is obtained from the average of more than 1000 of bubble images in a time series. Note that each image has 8 bits of dynamic range of light intensity.

(2) By subtracting the background image from each original images, only the bubble-like objects can be detected. By applying this process, the bubbles that are out of focal plane are not visible, or the objects become small.

(3) By using a certain threshold level of light intensity, the bubbles in focal plane images are binary (black–white). These images are filtered through the median filter, and spurious single black pixels indicated bubble presences are removed.

(4) In order to prevent miss-recognition of overlapped bubbles as single bubbles, the roundness (given by $L^2/4\pi A$, where L and A are the circumference length and area of the object, respectively) is adopted. The irregular images are removed.

Our arrangement consists of two CCD cameras; one for PIV/LIF (left camera in Fig. 1) and the other (right camera) for detecting bubble shape. A square "window" within the array of LEDs provides optical access for PIV/LIF. In order to simultaneously capture both bubble shape and flow field, we synchronized the triggering of the laser, the LEDs and the two CCD cameras.

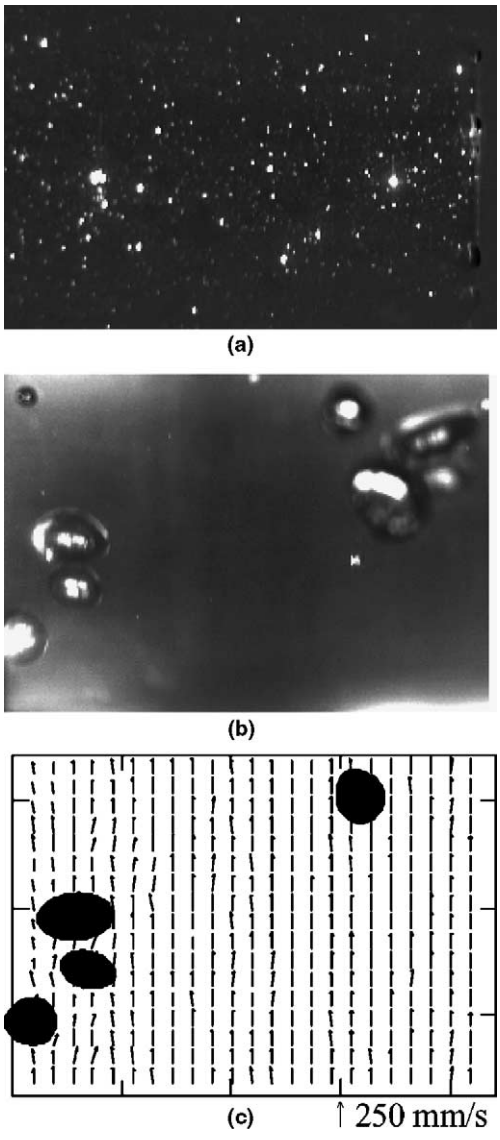

Fig. 2. Typical snapshots of bubbles and velocity vector field: (a) fluorescent tracer particles image, (b) bubble shadow image, (c) velocity vector field.

Fig. 2(a) and (b) shows typical snapshots taken by each camera simultaneously. Velocity vector field as shown in Fig. 2(c) is reconstructed using these images.

3. Experimental apparatus and conditions

Fig. 3 shows the schematic of the experimental apparatus and bubble generator. The experimental setup consists of lower and upper tanks, a vertical pipe in between them, a pump, and an air compressor. Tap water, the test fluid, was pumped upward in the pipe. At the bottom of the pipe there is an entrance section with a honeycomb plate and a converging nozzle, with about 15% of contraction area ratio to rectify the incoming flow. Upstream of the nozzle there is an air bubble

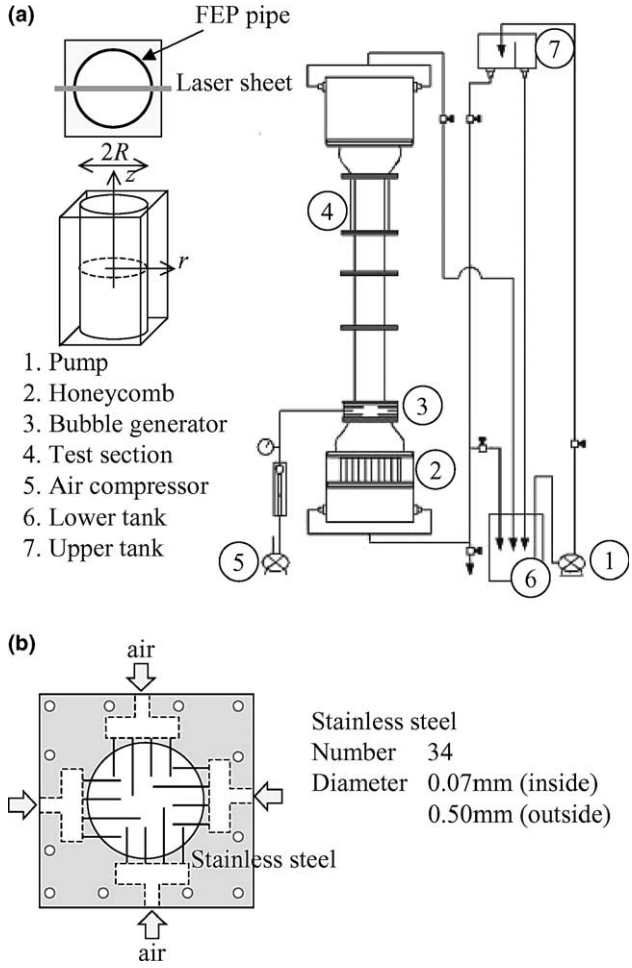

Fig. 3. Schematic of experimental setup: (a) experimental apparatus, (b) bubble generator.

generator. Fig. 3(b) shows a schematic of the bubble generator consisting of 34 stainless steel pipes with an inner and outer diameter of 0.07 and 0.50 mm, respectively. The air pressure and flow rate are controlled by a pressure gauge and flow meter.

The test section is a 1500 mm high acrylic pipe with an inner diameter, $2R$, of 44 mm. We applied an FEP pipe in the test section to avoid optical distortion due to refraction from the pipe. The refractive index of FEP material is approximately as the same as that of water. This has been done successfully by Hosokawa et al. (2000).

The center axis of pipe is defined as the origin. The upward flow direction is taken to be the positive z-axis and radial direction is taken to be the r-axis. The laser sheet for PIV illuminated the r–z plane.

Table 1 summarizes the experimental conditions. All the experiments are run at the bulk velocity of the single-phase flow $V_{sb} = 222$ mm/s, corresponding to a Reynolds number of 11,000 based on pipe diameter and bulk velocity ($Re_{2R} = 2RV_b/v$). In order to compare the effect of the bubble diameter with the same void fraction,

Table 1
Experimental conditions

Pipe diameter	$2R$	44 [mm]
Bulk velocity (single-phase)	V_{sb}	222 [mm/s]
Channel Reynolds number	Re_{2R}	11,000
Estimated friction velocity	v_τ	13.3 [mm/s]
Reynolds number	Re_τ	320
Void fraction	α	0.5% ($Q_g = 220$ ml/min)
	α	1.0% ($Q_g = 450$ ml/min)

Refractive index of FEP 1.338 np; water 1.333 np.

nearly 60 ppm of 3-pentanol ($C_5H_{11}OH$) was added as a surfactant, 3-pentanol prevents bubble coalescence. The effect of surfactant as a contaminate on the bubble surface increases the local shear rate in the vicinity of the bubble. It affects the bubble drag force especially in the case of small bubbles, less than 100 of bubble Reynolds number (Takemura and Magnaudet, 2003). In this study, the bubble Reynolds number is over 100, and a shedding vortex and/or the large wake, induced by the bubble shape is observed behind the bubbles. The effect of surface tension of bubble is considered to be small in this flow condition. Consequently, the turbulence modification can be examined for different bubble size. An additional advantage of the surfactant 3-pentanol has a negligible effect on the average void fraction. This is demonstrated by Fig. 4 showing the probability density function of area equivalent bubble diameter D_{eq}, i.e. the diameter of a circle having the same area as the bubbles in two dimensions. D_{eq} is estimated from the projected bubble shadow image determined by image processing techniques. For the case without the surfactant, D_{eq} takes the peak value at about 2.0 mm. On the other hand with the surfactant, it takes the peak value at about 1.2 mm within a small dispersion. Hereafter, the cases without and with surfactant are referred to as $D_M = 2$ and 1 mm, respectively.

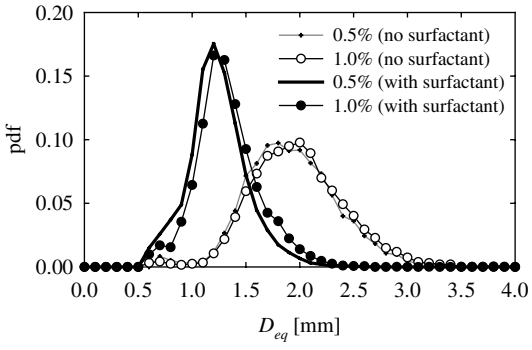

Fig. 4. Effect of 3-pentanol on pdf of equivalent bubble diameter D_{eq}.

4. Results and discussion

4.1. Bubbly flow structure in the pipe

Fig. 5 shows the mean and the fluctuation velocity profiles in single-phase flow. Fully developed turbulent flow is observed at the measurement area, and there is no influence of the surfactant on the turbulent structure.

Instantaneous velocity vector fields in the time sequence with this measurement technique are shown in Fig. 2(c). White spots are denoted as the bubbles. Bubbles accumulate near the wall. In the middle pipe region, there are fewer bubbles and the liquid phase of the flow is undisturbed.

The average flow field is estimated from more than 1000 instantaneous velocity vector fields. Fig. 6 shows the streamwise mean velocity profile for both the liquid phase and dispersed bubbles. They are normalized by

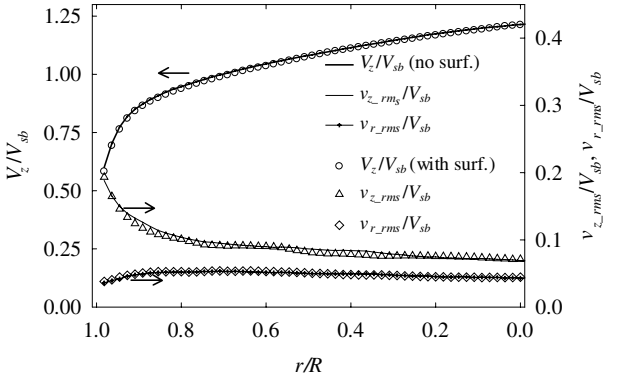

Fig. 5. Effect of 3-pentanol on single-phase flow.

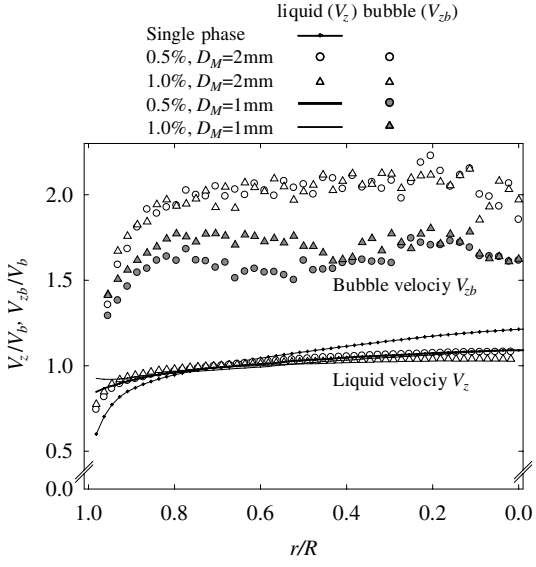

Fig. 6. Streamwise mean velocity of liquid phase V_z/V_b and bubble rising velocity V_{zb}/V_b profiles.

the bulk velocity V_b in each condition. According to the bubble velocity profiles, bubble phase is preceded by the liquid phase for whole pipe region. The liquid phase velocity V_z near the wall is larger than the single-liquid-phase velocity, and the mean streamwise velocity profile flatters (plug-like flow) for each condition. For the case of smaller diameter, V_z became more uniform in the vicinity of the wall. In this study at the middle pipe region, the average bubble velocity is more than 1.5 times larger than the liquid phase velocity, although Fig. 6 shows no significant effect of bubble size on the liquid phase mean velocity.

In Fig. 7, the local void fraction α_l profile is estimated. Here, α_l is defined as the ratio of the bubble volume to the measurement volume for each r position. The bubble cross section in the perpendicular plane to r–z plane is assumed to be a circle with the same diameter as a chord of the bubble in the z direction. We projected the given diameter of the acrylic sphere that is settling in the vessel with the same technique within an uncertainty of 20%.

According to the local void fraction profile, bubbles accumulate near the pipe wall ($r/R > 0.9$), and α_l became high in this area for each case. The profile of α_l depends on both the mean void fraction and the addition of the surfactant. The local void fraction α_l takes peak value at about $r/R = 0.9$ for large bubble diameter $D_M = 2$ mm; on the other hand for smaller bubble the peak appeared at approximately $r/R = 0.95$. It is expected that lateral bubble motion near the wall is dominated by the shear induced lift force (Auton, 1987), which consists of the bubble slip velocity and the flow circulation around the bubble. The bubble slip velocity influences the lift force significantly, such that small bubbles tend to move toward the wall in this experiment. The local void fraction α_l peaks relatively closer to the wall for a small bubble diameter D_M. Note that α_l peaks at nearly the same distance from the wall as D_M. This trend is in good agreement with the experiments conducted by Serizawa et al. (1975). Moreover the effect of difference of bubble number density appears as the intensity of α_l for a given D_M.

Including the effects of local void fraction, bubbles that ascended in the vicinity of the wall accelerate the liquid phase flow near the wall. Especially for the case with small D_M, most of the bubbles ascend in the region, $r/R > 0.95$, thus average streamwise velocity of liquid V_z in this region is larger than that in the case with large diameter. However the small local void fraction has less influence on average liquid phase flow structure in the middle pipe region, the mean streamwise velocity becomes flat.

5. The effects of bubbles on turbulence modification

Fluctuation velocity profiles are shown in Fig. 8. In this study the streamwise fluctuation velocity v_{z_rms} is mainly suppressed. Although near the wall ($r/R > 0.9$), v_{z_rms} has nearly same or larger intensity than that in single-phase flow in the large bubble case ($D_M = 2$ mm). Wake structure and the local shear flow induced by large bubbles accumulating near the wall enhance the fluctuation velocity. This is suppressed rapidly in the middle pipe region, and turbulent intensity is reduced. On the other hand in the case of small bubbles ($D_M = 1$ mm), v_{z_rms} is suppressed rapidly in $\alpha = 1.0\%$. The turbulence intensity is reduced when the large number of bubbles ascend in the vicinity of the wall.

According to fluctuation velocity profiles in the radial direction v_{r_rms}, turbulence is enhanced near the wall, and the enhanced region depends on bubble diameter D_M. This region is nearly the same as the higher local void fraction region. The fluctuation velocity in radial direction is induced by lateral migration of bubbles. For small bubbles v_{r_rms} profiles have a similar shape to

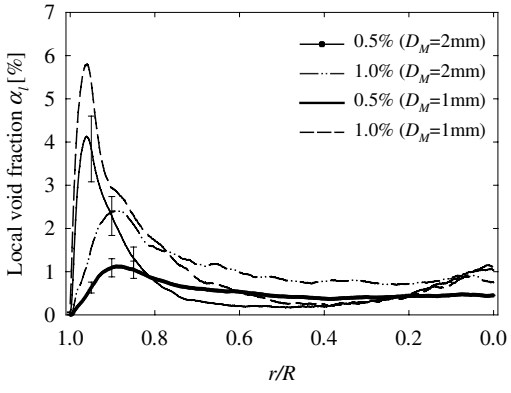

Fig. 7. Local void fraction profile.

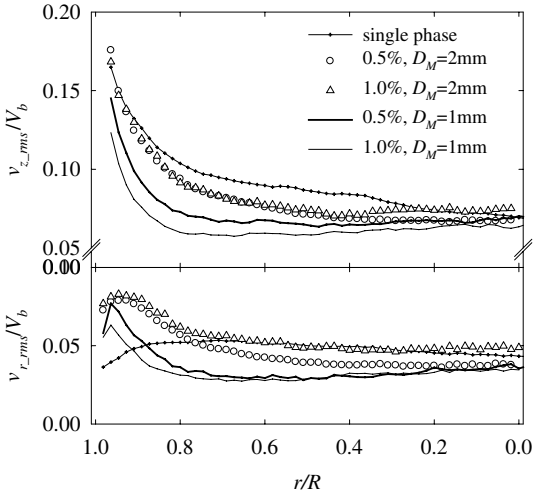

Fig. 8. Fluctuation velocity profile of liquid phase in streamwise v_{z_rms} and radial direction v_{r_rms}.

v_{z_rms} profiles. Large number density of small bubbles ($\alpha = 1.0\%$) near the wall induces reduction of turbulence intensity. On the other hand for the large D_M, v_{r_rms} is enhanced at the higher local void fraction ($\alpha = 1.0\%$). In this condition the local void fraction near the wall is larger than in other cases. The wake induced by large number of larger ascending bubbles entrains surrounding fluid and increases the radial fluctuations. In the middle pipe region, v_{r_rms} is suppressed rapidly.

6. Turbulence energy budget of liquid phase and instantaneous vortical structure around the bubbles

The effect of bubbles on the turbulence energy budget should be discussed. The equation for the kinetic energy ($\langle v_i' v_i' \rangle/2$) of turbulence in bubbly flow is written as

$$\frac{\mathrm{D}(1-\langle\alpha_\mathrm{l}\rangle)\langle v_i' v_i'/2\rangle}{\mathrm{D}t} = P_{ii} + T_{ii} + D_{ii} + \Pi_{ii} + \varepsilon_{ii} + E_{ii} \quad (1)$$

where $\langle\,\rangle$ is defined as the time average value. The terms on the right-hand side of Eq. (1) are: turbulence energy production, P_{ii}, turbulent diffusion, T_{ii}, viscous diffusion, D_{ii}, pressure gradient work, Π_{ii}, dissipation, ε_{ii}, and external force, E_{ii}. The most effective elements of production and dissipation terms of pipe flow are estimated by

$$P_{ii} \approx -(1-\langle\alpha_\mathrm{l}\rangle)\langle v_r' v_z'\rangle \frac{\mathrm{d}V_z}{\mathrm{d}r}, \quad (2)$$

$$\begin{aligned}\varepsilon_{ii} &\approx \frac{1}{2}\nu(1-\langle\alpha_\mathrm{l}\rangle)\left(\left\langle v_i'\frac{\partial^2 v_i'}{\partial x_\mathrm{l}\partial x_\mathrm{l}}\right\rangle + \left\langle v_i'\frac{\partial^2 v_i'}{\partial x_\mathrm{l}\partial x_\mathrm{l}}\right\rangle\right)\\ &= \nu(1-\langle\alpha_\mathrm{l}\rangle)\left(\left\langle v_r'\frac{\partial^2 v_r'}{\partial r\partial r}\right\rangle + \left\langle v_r'\frac{\partial}{\partial x_\theta}\left(\frac{1}{r}\frac{\partial v_r'}{\partial\theta} - \frac{v_\theta'}{r}\right)\right\rangle\right.\\ &\quad + \left\langle v_r'\frac{\partial^2 v_r'}{\partial z\partial z}\right\rangle + \left\langle v_\theta'\frac{\partial^2 v_\theta'}{\partial r\partial r}\right\rangle + \left\langle v_\theta'\frac{\partial}{\partial x_\theta}\left(\frac{1}{r}\frac{\partial v_\theta'}{\partial\theta} - \frac{v_r'}{r}\right)\right\rangle\\ &\quad + \left\langle v_\theta'\frac{\partial^2 v_\theta'}{\partial z\partial z}\right\rangle + \left\langle v_z'\frac{\partial^2 v_z'}{\partial r\partial r}\right\rangle + \left\langle v_z'\frac{\partial}{\partial x_\theta}\left(\frac{1}{r}\frac{\partial v_z'}{\partial\theta}\right)\right\rangle\\ &\quad \left. + \left\langle v_z'\frac{\partial^2 v_z'}{\partial z\partial z}\right\rangle\right). \end{aligned} \quad (3)$$

Eq. (2) is adopted as the most dominant term for dissipation rate (Elghobashi and Abou-Arab, 1983). It is assumed that the flow is axis-symmetry and the velocity gradient for angular direction (θ) is negligibly small such that

$$v_\theta' \approx 0, \quad \frac{\partial v_r'}{\partial\theta} \approx 0, \quad \frac{\partial v_z'}{\partial\theta} \approx 0. \quad (4)$$

Thus, the dissipation term may be approximated by

$$\begin{aligned}\varepsilon_{ii} \approx \nu(1-\langle\alpha_\mathrm{l}\rangle)\left(\left\langle v_r'\frac{\partial^2 v_r'}{\partial r\partial r}\right\rangle + \left\langle v_r'\frac{\partial^2 v_r'}{\partial z\partial z}\right\rangle\right.\\ \left. + \left\langle v_z'\frac{\partial^2 v_z'}{\partial r\partial r}\right\rangle + \left\langle v_z'\frac{\partial^2 v_z'}{\partial z\partial z}\right\rangle\right). \end{aligned} \quad (5)$$

As shown in the former investigation (Maxey and Riley, 1983; Magnaudet, 1997), there are many factors contributing to the force acting on bubbles, for example drag force, added mass force and pressure gradient force. Here, the force represented by the extra force term, E_{ii}, is a drag force based on the relative velocity of the bubble and its projected diameter (Druzhinin and Elghobashi, 1998). A rough estimation of E_{ii} is given by

$$E_{ii} \approx -\langle\alpha_\mathrm{l}\rangle\langle F_i'\rangle\langle v_i'\rangle, \quad (6)$$

where α_l is local void fraction, F_i' is the fluctuation of the force affected by bubbles, and v_i' is the liquid phase fluctuation velocity.

Fig. 9 shows turbulence energy production and dissipation profiles, here the effect of bubble diameter is compared for each condition. The production is governed by the average shear rate $\partial V_z/\partial r$. In addition to the flat profile of streamwise mean velocity V_z, Reynolds stress profile is rapidly suppressed, thus the production term became remarkably small in bubbly flow. Especially in case of small D_M, profile becomes flatter due to the flat profile of V_z accelerated by bubbles accumulating near the wall. In the vicinity of wall, high intensity of the average shear rate induces turbulence energy production, while there is no production in the middle pipe region.

Fig. 10 shows the mean vorticity profile for $\alpha = 0.5\%$ compared with the effect of bubble diameter D_M. The vorticity ω is defined in terms of that circulation and calculated using the following equation in order to prevent the error propagation from the differentiation of experimental data.

$$\begin{aligned}\omega_{0,0} \equiv (&-v_{r1,1}\Delta r - v_{r0,1}\Delta r - v_{z-1,1}\Delta z - v_{z-1,0}\Delta z\\ &+ v_{r-1,-1}\Delta r + v_{r0,-1}\Delta r + v_{z1,-1}\Delta z\\ &- v_{z1,0}\Delta z)/(4\Delta r\Delta z), \end{aligned} \quad (7)$$

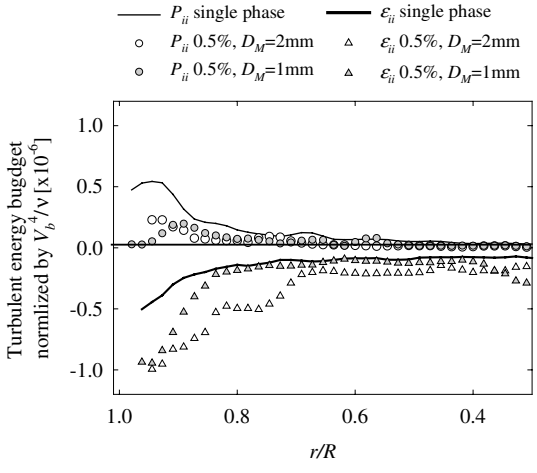

Fig. 9. Turbulent energy budget of liquid phase.

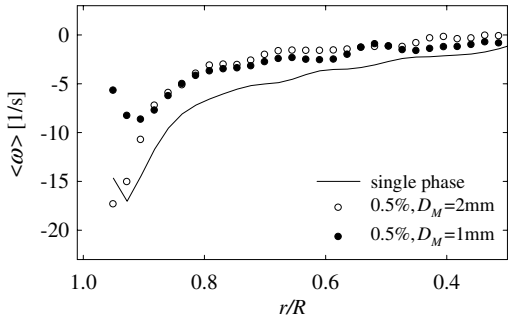

Fig. 10. Mean vorticity profile of liquid phase in $\alpha = 0.5\%$.

where Δr and Δz are the distance between each point of data in r, z direction. For a large bubble, the average vorticity $\langle\omega\rangle$ takes nearly the same or barely enhanced values as compared to single-phase flow near the wall. On the other hand for small D_M, the intensity of $\langle\omega\rangle$ is smaller than that for single-phase flow. These results suggest that the large scale flow structure, i.e. mean velocity gradient near the wall, becomes flatter due to the ascending small bubbles, accordingly the $\langle\omega\rangle$ becomes flatter for this case as compared to that of single-phase flow. The effect of eddies induced by the wake of small bubbles are not reflected by the averaged quantities.

The dissipation profile in Fig. 9 indicates an energy sink. The quantity of ε_{ii} is plotted to discuss the effect of bubbles on turbulence energy budget. Dissipation has higher value near the wall for each condition, and in the bubbly flow these are increase the energy sink in the whole region. Especially near the wall it increases remarkably compared to the single-phase flow case.

In order to clarify the effect of local flow structure around the bubbles, the instantaneous fluctuation vorticity intensity Ω defined by

$$\Omega = (\omega - \langle\omega\rangle)^2 \tag{8}$$

is examined. A high fluctuation vorticity intensity Ω is expected to stretch a vortex string and cascade it into small scale eddies, thus Ω has a strong correlation to turbulence energy dissipation (Tennekes and Lumley, 1972). Fig. 11 shows typical instantaneous Ω contours for two different bubble diameters at $\alpha = 0.5\%$. In Fig. 11 high intensity of Ω appears in the region around the bubble. In particular in Fig. 11(a) the high intensity region appears not only in the wake region but also in the inter-bubble spacing. On the other hand in Fig. 11(b), the bubbles accumulate in the vicinity of the wall, thus the flow accelerates by the bubbles and wall interacts in the high intensity of Ω. There appears a smaller uniform distribution of Ω in the middle pipe region. It indicates that significant energy dissipation occurs between the wall and bubbles. The high intensity of Ω is more widely spread in the large bubble case than that in the small bubble case. Since the length scale of high

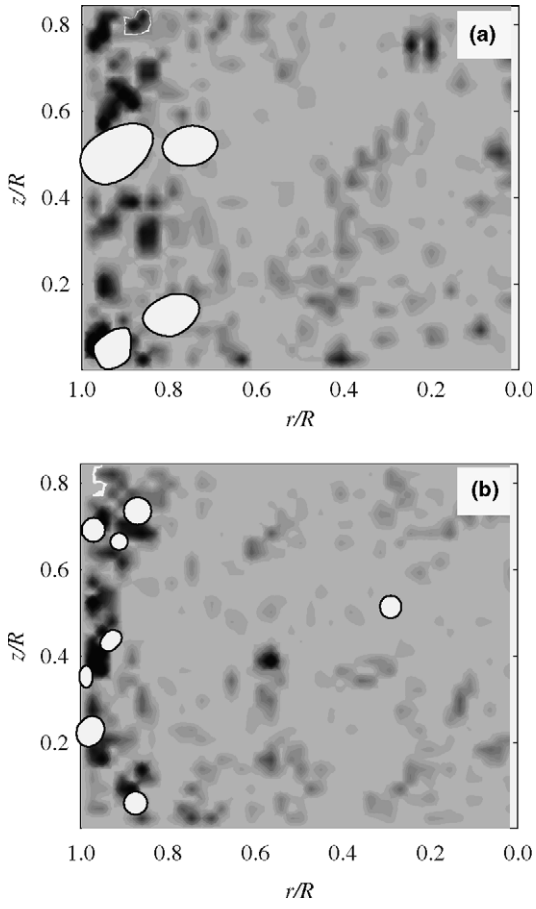

Fig. 11. Instantaneous fluctuation vorticity intensity Ω [1/s^2] contours: (a) $\alpha = 0.5\%$, $D_M = 2$ mm, (b) $\alpha = 0.5\%$, $D_M = 1$ mm.

intensity of the vorticity is nearly the same as the bubble diameter, a high intensity of Ω appears in the region far from the wall no matter how closely the bubble ascends near the wall. Additionally the distance depends on the bubble diameter and the large bubbles ascend not only in the near wall region but also in the middle-pipe region as shown in Fig. 7.

It can be expected that the bubble wake induced turbulence energy dissipation directly for these conditions.

The production and dissipation terms in this bubbly flow are not in complete energy balance as other contributions produce turbulent energy. The energy containing eddy length scale D_{es} is estimated as $D_{es} = 1.5$–2.0 mm in both conditions, that is nearly 1 to 2 times larger than the bubble diameter. It suggests that an effective of energy production is the force effected by bubbles, E_{ii}. The former researchers have attempted to include this term. They estimated the influence of the force acting on the particles or bubbles and particle loading density or void fraction (Elghobashi and Megahed, 1981; Elghobashi and Abou-Arab, 1983; Druzhinin and Elghobashi, 1998).

By an estimate of E_{ii} ($\alpha = 0.5\%$), a drastic distinction between bubble diameter $D_M = 1$ and 2 mm is recognized. In the middle pipe region, both value are the same order of P_{ii}, i.e. O(0.1–1). While in the vicinity of the wall, E_{ii} increases toward the wall. In case of large bubbles, the order of E_{ii} is nearly O(0.1–1), and it is O(1–10) in small bubble condition. The difference of these two values is from the profile of local void fraction. The drag force on an individual bubble is small, more than 4 times the local void fraction near the wall. This induces the extra force on the liquid phase resulting in the gain of turbulent energy.

This suggests that the accumulated bubbles in the vicinity of the wall accelerate the liquid phase, and induce turbulence energy production in this region, while the local flow structure around the bubbles affects the turbulent energy dissipation directly.

7. Conclusions

The experimental investigation of vertical pipe flow injected with dispersed bubbles has been conducted using PIV/LIF, and projecting shadow image technique. For the case of a high void fraction in the vicinity of the wall, average streamwise velocity profile becomes flat, and turbulence intensity and Reynolds stress are dramatically reduced in a wide region of the pipe. The enhanced region of turbulent intensity depends on the bubble diameter, i.e., this region is nearly the same as the higher local void fraction region.

From the statistical value of turbulence properties estimated by the instantaneous velocity vector fields obtained by PIV measurement, the following mechanisms are suggested for the turbulence energy production and dissipation. The production term is nearly zero because the mean velocity becomes flat from the accumulation of bubbles and mean velocity gradient is negligibly small. However the external force effected by bubbles is expected to contribute the turbulence energy production. The turbulence energy dissipation occurs around the bubble due to bubble-induced eddies, that is confirmed by estimation of the fluctuation vorticity intensity value.

Acknowledgements

This research was carried out as part of the research activity at the Center for Smart Control of Turbulence and funded by MEXT. The first author expresses her gratitude to Mr. Tanaka for conducting the experiment, assisting in the data analysis and helpful discussions.

References

Auton, T.R., 1987. The lift force on a spherical body in a rotational flow. J. Fluid Mech. 183, 199–218.

Bunner, B., Tryggvson, G., 2002. Dynamics of homogeneous bubbly flows, Part 2. Velocity fluctuations. J. Fluid Mech. 466, 53–84.

Bunner, B., Tryggvson, G., 2003. Effect of bubble deformation on the properties of bubbly flows. J. Fluid Mech. 495, 77–118.

Druzhinin, O.A., Elghobashi, S., 1998. Direct numerical simulations of bubble-laden turbulent flows using the two-fluid formulation. Phys. Fluids 10 (3), 685–697.

Elghobashi, S.E., Abou-Arab, T.W., 1983. A two-equation turbulence model for two flows. Phys. Fluids 26 (4), 931–938.

Elghobashi, S.E., Megahed, I.E.A., 1981. Mass and momentum transport in a Laminar isothermal two-phase round jet. Numer. Heat Transfer 4, 317–329.

Hosokawa, S., Takesaka, K., Tomiyama, A., Kondo, Y., 2000. LDV measurement of Reynolds stresses in gas–liquid two-phase bubbly flow in a vertical pipe. In: 2nd Japan–Korea Symposium on Nuclear Thermal Hydraulics and Safety. Fukuoka, Japan, October 15–18, pp. 247–252.

Lain, S., Bröder, D., Sommerfeld, M., Göz, M.F, 2002. Modeling hydrodynamics and turbulence in a bubble column using the Euler–Lagrange procedure. Int. J. Multiphase Flow 28, 1381–1407.

Lance, M., Bataille, J., 1991. Turbulence in the liquid phase of a uniform bubbly air–water flow. J. Fluid Mech. 222, 95–118.

Magnaudet, J., 1997. The forces acting on bubbles and rigid particles. ASME FED Summer Meeting, CD-ROM.

Maxey, M.R., Riley, J.J., 1983. Equation of motion for a small rigid sphere in a non-uniform flow. Phys. Fluid 26, 883–889.

Murai, Y., Song, X., Takagi, T., Ishikawa, M., Yamamoto, F., Ohta, J., 2000. Inverse energy cascade structure of turbulence in a bubbly flow (PIV measurement and results). JSME Int. J., Series B 43 (2), 188–196.

Sato, Y., Hishida, K., 1996. Transport process of turbulence energy in particle-laden turbulent flow. Int. J. Heat Fluid Flow 17, 202–210.

Sato, Y., Hishida, K., 2000. Effect of inter-particle spacing on turbulence modulation by Lagrangian PIV. Int. J. Heat Fluid Flow 21, 554–561.

Serizawa, A., Kataoka, I., Michiyoshi, I., 1975. Turbulence structure of air–water bubbly flow—II. Local properties. Int. J. Multiphase Flow 2, 235–246.

Takemura, F., Magnaudet, J., 2003. The transverse force on clean and contaminated bubbles rising near a vertical wall at moderate Reynolds number. J. Fluid Mech. 495, 234–253.

Tennekes, H., Lumley, J.L., 1972. A First Course in Turbulence. MIT Press, Cambridge, Mass.

Theofanous, T.G., Sullivan, J., 1982. Turbulence in two-phase dispersed flows. J. Fluid Mech. 116, 343–362.

Tokuhiro, A., Maekawa, M., Iizuka, K., Hihsida, K., Maeda, M., 1998. Turbulent flow past a bubble and ellipsoid using shadow-image and PIV techniques. Int. J. Multiphase Flow 24, 1383–1406.

Wang, S.K., Lee, S.J., Jones Jr., O.C., Lathey Jr., R.T., 1987. 3-D turbulence structure and phase distribution measurements in bubbly two-phase flows. Int. J. Multiphase Flow 13 (3), 327–343.